International Journal for Housing Science and Its Applications
Publish August 3, 2025. Volume 46, Issue 3 Pages 155-169

https://doi.org/10.70517/ijhsa46311

Three-dimensional modeling and localization method for safety distance of power line based on hierarchical algorithm and visual sensor

Fei Shen[1,*], Yurong Zhang[1] and Bin Qian[1]
[1] State Grid Jiangsu Electric Power Co., Ltd. Taizhou Power Supply Branch, Taizhou, Jiangsu, 225300, China
Corresponding authors: (e-mail: qianbin0320@163.com).

Abstract The implementation of traditional energized line operation relies on manual experience, which has the problems of outdated control technology and insufficient reliability, and seriously affects the operation safety. In this paper, based on the hierarchical algorithm and visual sensor, after completing the preprocessing of the visual sensor data, the point cloud data is combined with the power line operation to obtain the point cloud data characteristics under the power line operation scene. At the same time, a point cloud alignment method based on octree and KD tree multilayer index structure is proposed to improve the traditional ICP point cloud alignment algorithm for three-dimensional modeling of the safety distance of power line. Then the safety distance of the power line operation is calculated to realize the safety distance localization of the power line by visual sensors. Compared with the traditional BIM and GIM modeling methods, the 3D model elevation point location curve under the modeling method of the safety distance of the power line in this paper has a higher degree of fit with the original curve and higher modeling accuracy. The safety distance localization method of energized lines in this paper also meets the safety distance warning requirements of 10kV and 35kV voltage levels at the same time, and the validity has been verified.

Index Terms point cloud data, octree, KD tree, visual sensor

I. Introduction

In terms of the electric power industry, high-voltage transmission lines have become the arteries of the national economy, guaranteeing the normal operation of the daily activities of many industries, and also carrying the basic electricity needs of the people, so once the high-voltage transmission lines are shut down due to faults, it will result in huge economic losses and unpredictable social impacts [1]-[3]. Therefore, how to maintain and overhaul high-voltage transmission lines with fewer power outages or without power outages (i.e., charged operation) and make them intelligent with the development of technology has become an important research direction. In 2021, State Grid deepened the construction of intelligent operation and inspection system, continued to promote the deep integration and application of modern information and communication technology, digital twin technology, control technology and energy technology, to enhance the ability of grid-wide sensing and flexible control, optimize the shift operation mode and equipment management mode as the goal, to formulate and put forward a continuous strengthening of the equipment operation and inspection of the digital shift construction, and other specific work programs and implementation requirements, to improve the stability of grid operation [4]-[7]. In 2019, the State Grid Corporation also clearly put forward the specific requirements to continuously improve the level of active safety protection at the operation site, deepen the application of helicopters, robots and drones, and other intelligent equipment in the auxiliary power-carrying operation work, and carry out the refinement and intellectualization of the various operations of power-carrying operation [8]-[10]. Energized operation is an important means of electric equipment testing, overhaul and maintenance and transformation and upgrading, and it is an important technical basis for ensuring the reliable operation of the power grid [11]. And due to the high voltage level of the transmission line, the operator, after entering the electric field, in order to ensure their own safety need to maintain a certain safety distance from the charged body, this can ensure the safety of the energized operation personnel, the minimum air gap distance is the minimum safety distance [12].

In the early stage of power-carrying operation, manual measurement of the safety distance of power lines is a method that is used very frequently, but the method has obvious defects such as low efficiency, large error, high risk, and great influence by weather and environment. At present, with the continuous growth of the scale of transmission lines and the popularization and application of intelligent inspection technology means, the traditional mode of power-carrying maintenance operation mode in terms of safety control and technical level obviously does

not meet the actual demand for power-carrying operation [13]. Lei et al [14] conducted a helicopter strip operation test of the suspension method on transmission lines, which clarified the safety distance of ±400kV DC transmission operators and realized a low-risk strip operation environment of 10-5. However, the cost of this method is high and the environmental interference is serious. Zhang et al [15] proposed a simulation calculation method for safe distance of electric work based on the type of tower and line condition, which was calculated by cupola and suspension basket mode for the environmental voltage and electric field strength of the operator, and the safe distance location was determined. Ruan et al [16], in their design of an early warning system for detecting and detecting the high voltage line electric work, utilized a time-of-flight depth camera to measure the safe distance for energized work to obtain positioning information. The measurement is based on real-time environment, but the camera is expensive and the accuracy of the measurement is reduced in rainy and foggy environments. Li et al [17] introduced China's Beidou III system to carry out real-time safety distance calculation and positioning of power-carrying workers through the calculation of point cloud data in the three-dimensional model of 220kV transmission lines, which not only optimizes the calculation efficiency, but also covers the improvement of the accuracy of positioning. Wu et al [18] designed a PointMGA segmentation model based on PointNet++, which acts on the point cloud data in the bandwidth operation environment and combines with the farthest point sampling-dichotomous area growth distance algorithm to determine the hazardous area of bandwidth operation, which laterally provides the location of the safe distance of the operation. Wang et al [19] performed 3D modeling of the overhead line power-carrying operation site by an improved two-way filtering algorithm, collected the 3D model point cloud data by LiDAR, determined the safety distance of individual points by an octree-nearest-point search algorithm, and combined with the actual safety distance regulations to obtain the safety distance localization for power-carrying operation. Li et al [20] created a monocular vision method for automatic measurement of electrically charged safety distances, specifically from the use of instance segmentation, depth estimation, and inverse projection techniques to calculate the distance of a two-dimensional object in a three-dimensional environment, and based on the point cloud data of the object in the three-dimensional environment as well as the ratio of the conversion of the two-dimensional and three-dimensional distances to calculate the safety distances, which was measured with an error of less than 9%. In most of these studies, the point cloud data of the 3D model is utilized for the localization work, but it does not exclude the influence of the dynamic environment interference on vision, machine equipment, and intelligent algorithms. The development of visual sensor technology, under the premise of meeting human needs for visual perception, provides more convenient and efficient way of working for human beings, regardless of the distance from the target of several meters or centimeters away, through the sensor can see the delicate target image, which helps to improve the accuracy of the data under the environmental interference [21].

In this paper, a three-dimensional laser scanning system is used to collect point cloud data, and the processing of point cloud data of the energized line is realized through the methods of coarse difference rejection and point cloud classification. Aiming at the low efficiency of KD tree multidimensional query in point cloud alignment algorithm, a point cloud alignment method based on octree and KD tree multilayer index structure is proposed. An octree global index is established for the model point cloud data, and then a KD tree index is constructed for the local data at the leaf nodes of the octree. The global index values of the leaf nodes are used to quickly locate the local point cloud data blocks, the local KD tree index is used to speed up the search of the nearest point, and the Euclidean distance threshold, point-to-point distance difference and normal vector threshold are used to eliminate some noise points when calculating the nearest point. Finally, the distance of each line point to each equipment point is calculated by traversing, and the part which is smaller than the threshold value is taken to calculate the safety distance of the live line, and the efficiency of spatial search for the nearest point is improved by utilizing the KD-tree search to realize the positioning of the safety distance of the live line. Carry out the experiments of modeling and positioning of the safety distance of the power line separately to test the effectiveness of the three-dimensional modeling and positioning method of the safety distance of the power line based on the visual sensor proposed in this paper.

II. Multi-data fusion and noise reduction processing for visual sensors

Before the three-dimensional modeling and localization of the safety distance of the power line, this chapter will firstly fuse the visual sensor multiple data, de-noise the inspection visual information through the compressed perception method, and complete the pre-processing work of the visual sensor data.

II. A. Visual Sensor Multi-Data Fusion

Visual sensors include different types of cameras or infrared cameras, which can provide rich visual information [22]. By fusing the data from multiple visual sensors, the image data of the line can be obtained from different angles and fields of view, which can increase the comprehensive knowledge and recognition ability of the line defects. First

of all, the fusion of multi-vision sensor data can improve the reliability and accuracy of line inspection. As different types of sensors have different sensitivities to light, color and texture, the image information obtained will be different. By comparing and correcting the data from multiple sensors, the possibility of misjudgment and omission can be reduced, and the detection accuracy of line defects can be improved. Secondly, the fusion of multi-vision sensor data can enhance the ability of image processing and analysis. The data provided by different visual sensors are diversified, including visible light, infrared, thermal image and other different spectral information. Combining these data for image processing and analysis can better identify the defects of overhead lines, such as insulation breakdown, conductor breakage, etc., and at the same time, some interference and noise factors are excluded to improve the robustness and reliability of the algorithm.

II. B.Denoising of inspection visual information

Noise is an irrelevant or disruptive component introduced during data acquisition, transmission and processing. During the inspection process, the visual information may be noisy due to the following reasons. In this section, denoising of overhead line visual information is realized by compressed perception method. Compressed perception is a theory and technique based on signal sparsity, which takes advantage of the sparsity of signals in low-dimensional representations to reconstruct high-quality signals with fewer measurement samples. In the denoising process of overhead line visual information, the compressed perception method is able to utilize the sparsity of the image, i.e., only some of the pixels in the image contain useful information, while the other pixels can be represented by a combination of this useful information. By compressed-aware sampling of overhead line images, the amount of data collected can be significantly reduced, and the overhead of storage and transmission can be reduced. In addition, the compressed-aware method can also achieve noise reduction by appropriately selecting a suitable measurement matrix, optimizing the design for the sparse characteristics of the overhead line image, and skipping the information that contributes less to the denoising process. Compared with the traditional image denoising methods, the compression-aware method better suppresses the noise and improves the denoising effect while maintaining the image quality.

III. Charged line safety distance three-dimensional modeling methods

3D reconstruction has a wide range of applications in computer vision, virtual reality, 3D printing and reverse engineering, etc. The advantages and disadvantages of the point cloud data alignment method directly affect the effect of 3D reconstruction [23]. In this chapter, based on the preprocessing data of the visual sensor, the point cloud data alignment method will be used to realize the three-dimensional modeling of the safety distance of the power line for the visual sensor.

III. A. Visual Sensor Point Cloud Data Processing

III. A. 1) Three-dimensional laser scanning technology

1) Point cloud data acquisition principle

The point cloud data acquired for power transmission and banding operation is later processed automatically or manually by software, and then the high-resolution digital image data is acquired, which can realize large-scale, high-precision and high-efficiency three-dimensional scene data measurement for dangerous environments and areas and parts that are difficult for distance measurement. At present, it can be categorized into three types according to the differences in principle: pulse-based ranging, phase-based ranging and triangular wave-based ranging.

(1) Pulse Ranging

Pulse ranging is a method that realizes distance measurement by calculating the flight time of the laser. The laser source utilized in this method to carry out three-dimensional point cloud data acquisition for power transmission banding operations has the remarkable features of fast speed, very short duration, high instantaneous power of emission, and high degree of energy concentration. Available:

$$D = \frac{1}{2} c \cdot t \tag{1}$$

Where: t denotes the round trip time of the laser pulse, c denotes the velocity of the laser in the air, and D denotes the distance between the radar and the point to be measured.

From equation (1), the error transfer equation (2) is given as:

$$\Delta D = c \cdot \Delta t \tag{2}$$

where: ΔD denotes the accuracy of the laser pulse ranging, and Δt denotes the accuracy of the time measurement, due to Eq. (2) it can be concluded that ΔD is only related to Δt. The maximum measurement distance $D_{\max}$ that can be realized is:

$$D_{\max} = \frac{1}{2} c \cdot t_{\max} \tag{3}$$

(2) Phase Ranging

Phase ranging is an important method used for laser ranging. The measured distance between the measuring point and the object to be measured is:

$$D = \frac{\lambda}{4\pi} \cdot \Delta\varphi \tag{4}$$

where: λ is the wavelength of the continuous wave and $\Delta\varphi$ is the phase difference between the transmitted wave and the received return wave.

(3) Triangulation

Triangulation is a way to obtain the distance between the measuring point and the object to be measured through the triangular geometric relationship. The laser transmits a series of laser pulses to the tower equipment and the surrounding environment to be measured, and the laser is reflected when it reaches the tower equipment and the objects in the surrounding environment, and then a CDD digital camera is used to receive the reflected wave signal at the other end of the baseline. Through the incident wave, the angle between the reflected wave and the length of the baseline between the laser point and the camera, the distance between the measurement point and the tower equipment and the surrounding environment is calculated using triangular geometric relationships.

(2) Point cloud data acquisition method

Three-dimensional laser scanning system is mainly used for power transmission site three-dimensional point cloud data acquisition, processing and application of professional systems, is based on three-dimensional LiDAR technology, with other equipment, devices, technology and related algorithms combined with a point cloud data measurement system. Three-dimensional laser scanning system according to the mode of operation, carrying the main body, equipment configuration and specific use requirements can be divided into the ground station laser scanning system, unmanned aircraft and other airborne laser scanning system, as well as vehicle-mounted laser scanning system specially used for the urban environment and transportation of the three types of laser scanning system.

III. A. 2) Point Cloud Data Acquisition for Transmission Banding Operations

Through a non-contact way, the point cloud data of the site with an error of only millimeters within 100 meters can be obtained for the safety analysis of the site of the power strip operation. Compared with the traditional way, the use of terrestrial laser scanning system avoids the problem of wrong results due to the inconsistency between drawings and the actual site, improves the safety of the operation, shortens the operation time, and the data is highly reliable, easy to operate, and is not affected by the meteorological conditions at the site. Combined with the actual site, the main attention in the point cloud data acquisition process is paid to the following aspects:

1) Considering the impact of water vapor, dust and other substances, the actual propagation speed of the laser in the air is less than the speed of light, increase the air dielectric constant correction ε, the corrected distance calculation formula is:

$$D = \frac{1}{2} \frac{c}{\varepsilon} t \tag{5}$$

2) Considering the impact of height difference, voltage level, transmission tower structure height varies, with reference to the radar device vertical scanning angle range of 120 ° attribute, and at the same time to avoid the problem of multi-point superposition of data after scanning directly to the tower, generally along the line toward the 45 ° ~ 60 ° frame scanning, and the bottom of the nearest point of the tower tower foot with the nearest distance from the device is as follows:

$$L \geq \frac{H}{\tan 60°} \tag{6}$$

where: L is the distance of the measurement point from the foot of the tower at the nearest point, and H is the distance from the ground line to the horizontal base.

III. A. 3) Transmission banding operation point cloud data processing

After the point cloud data acquisition is completed, this thesis adopts the data interpretation software supporting the ground laser measurement system, which only needs to import the acquired point cloud data, and then it can automatically interpret and generate the point cloud data under the geodetic coordinate system after alignment, and realize the organization and processing of the point cloud data synchronously.

1) Roughness rejection

Whether a point p in the point cloud is retained or not, the elevation Z' of this point can be interpolated by the points around it, and then the difference between the elevation Z and the elevation of the point p is calculated, which is larger than a certain limit ε and then rejected. Distance-weighted average interpolation is used in the paper. The specific formula is as follows:

The square of the distance d_i from the surrounding points to the point p:

$$d_i^2 = (x - x_i)^2 + (y - y_i)^2 \tag{7}$$

where: d_i is the distance from the surrounding point to the point p.

Distance weighting function:

$$c_i = 1 / (d_i^2 + e) \tag{8}$$

where: c_i denotes the distance weighted value and e is a constant.

The p point elevation interpolation:

$$Z_i = \sum_{i=1}^{n} c_i Z_i \Big/ \sum_{i=1}^{n} c_i \tag{9}$$

The point cloud rounding is done when $Z' - Z \geq \varepsilon$.

Where: Z' denotes the elevation of point i.

2) Point cloud classification

For the preliminarily processed 3D point cloud data of the transmission live operation site, it is necessary to further classify it, p_i and if the elevation difference dZ_i in p_i and the neighborhood containing the surrounding points is less than the set threshold value $Limit\_dZ$, and the slope $Slope_i$ is less than the given threshold value $Limit\_Slope$, then p_i is considered to be a ground point, otherwise, the point is considered to be a feature point. The specific classification functions are:

$$Po\,\mathrm{int}(p_i) = \begin{cases} 0, dZ_i < Limit\_dZ, Slope_i < Limit\_Slope \\ 1, else \end{cases} \tag{10}$$

where 0 indicates that the point cloud data are ground points and 1 indicates that the point cloud data are feature points.

Along the scanning line through the positive and negative directions of the collected point cloud data are processed and labeled in the above manner, and the combined results of the two scans are judged, if p_i point of $aiToR$ and $aiToL$ are both labeled with 0, then p_i is a ground point; if any one of $aiToR$ and 1 is labeled with 1, then p_i is a point of a ground feature. The specific determination expression for the above is specified as follows:

$$Po\,\mathrm{int}(P_i) = \begin{cases} 0, aiToR + aiToL = 0 \\ 1, else \end{cases} \tag{11}$$

Based on whether the elevation difference between the left and right points adjacent to it in the point cloud data and the point exceeds a given threshold, it is determined whether the point is a very low point, and if it is, it is rejected; otherwise, it is considered to be a feature point. Then, the slope and elevation difference are labeled to the left and right according to this already determined feature point. The specific algorithm is as follows:

The acquired point cloud data is divided into multiple scan lines along the Y axis, and the above method is used to find out the feature points in that scan line. The point cloud data within the scan lines are then labeled using a slope-based method for the data. The slope of two neighboring points is calculated as follows:

$$Slope_i = \frac{Z_i - Z_{i-1}}{\sqrt{\left(X_i - X_{i-1}\right)^2 + \left(Y_i - Y_{i-1}\right)^2}} \tag{12}$$

when the absolute value of the slope $Slope_i$ of point P_i satisfies the given threshold value $Limit\_Slope_i$, then determine the property of point p_i according to whether the point p_{i-1} is a ground point or not; otherwise, compute whether the elevation difference between point p_i and point p_{i-1}, D_z, satisfies the given threshold, and if satisfied, then it is a ground point, and the opposite is a ground point.

In addition, when the absolute value of the slope $Slope_i$ at point p_i does not satisfy the given threshold value $Limit\_Slope$.

When $Slope_i < 0$, the classification function is:

$$Po\,\mathrm{int}\left(P_i\right) = \begin{cases} 0, \left(P_{i-1} = 0, Z_i - Z_t < Limt_H\right) \\ \quad or\ \left(P_{i-1} = 1, Z_i - Z_t > Limt_H\right) \\ 1, \left(P_{i-1} = 0, Z_i - Z_t \geq Limt_H\right) \\ \quad or\ \left(P_{i-1} = 1, Z_i - Z_t \leq Limt_H\right) \end{cases} \tag{13}$$

where: Z_t is the elevation of the nearest ground point to the p_i point, and $Limt_H$ is the given elevation difference threshold.

For $Slope_i > 0$, the classification function can be:

$$Po\,\mathrm{int}\left(P_i\right) = \begin{cases} 0, P_{i-1} = 0, Z_i - Z_t < Limt_H \\ 1, P_{i-1} = 0, Z_i - Z_t \geq Limt_H \ or\ P_{i-1} = 1 \end{cases} \tag{14}$$

III. B. Visual sensor point cloud data alignment

III. B. 1) ICP algorithm for nearest point searching

The ICP algorithm establishes the corresponding point sets P and Q according to certain criteria, and calculates the optimal coordinate transformations, i.e., rotation matrices and translation vectors, to transform the point data in one coordinate system to another coordinate system by the least-squares iteration, and to minimize the error function [24]. Point cloud alignment can be regarded as the process of solving the transformation matrix, and the key to determining the coordinate transformation of the ICP algorithm lies in the ability to accurately and quickly find the nearest point of the point to be aligned in P in the model point cloud Q. Therefore, the main factor affecting the efficiency and accuracy of the ICP algorithm is the search method of the nearest point.

III. B. 2) Improvement of Nearest Neighbor Search Algorithm Based on KD Tree

Typically, calculating the nearest point of each point p in P requires calculating the Euclidean distance between p and all points in Q. The local KD tree is built for the point cloud data blocks of the leaf nodes of the octree, the octree of the model point cloud and the KD tree multilayer index can quickly locate the data block where the nearest point of p is located, and can avoid searching all the points [25]. The search process of the nearest point is divided into two steps: the first step searches the global index layer to locate the point cloud data block where the nearest point is located by searching the octree of the model point cloud, i.e., to find the leaf node of the octree containing the nearest point; the second step finds the corresponding root node of the KD tree according to the information stored in the leaf node of the octree, i.e., the KD tree storing the local data block, and then searches for nearest-neighborhood points in the local point cloud data block.

The main factor affecting the efficiency of nearest-neighbor search in a KD tree is backtracking, and the octree nodes store the relevant data information without backtracking to locate the local point cloud block containing the nearest-neighbor points. Each node in the octree corresponds to a spatial enclosing box, and according to the coordinates of the points to be aligned $p_i\left(x_i, y_i, z_i\right)$ and the spatial location and size of the enclosing box, the leaf nodes of the octree that need to be continued to search are determined. Let the spatial index value of the subcube where the nearest neighbor point $q_i\left(x_i, y_i, z_i\right)$ is located be (a, b, c), and the octree code of the node corresponding to the subcube be $q = q_{n-1} \cdots q_j \cdots q_1 q_0$, $q_j\left(j = 0, 1, \cdots, n-1\right)$ denotes the path from the leaf node to the root node. The global index value of the subcube where the nearest neighbor point in the octree is located can be obtained according to equation (15).

$$a=\sum_{j=1}^{n-1}\left(q_j\%2\right)\times 2^i$$
$$b=\sum_{j=1}^{n-1}\left(\left[\frac{q_i}{2}\right]\%2\right)\times 2^i \tag{15}$$
$$c=\sum_{j=1}^{n-1}\left(\left[\frac{q_i}{4}\right]\%2\right)\times 2^i$$

When searching for nearest-neighbor points in the local KD tree, for points located on the boundary of the segmented subunit, the search result may be wrong, and the boundary points can be treated as noise points, and due to the huge amount of data in the point cloud, such a treatment improves the speed of the alignment without much effect on the accuracy.

The improved algorithm utilizes Euclidean distance thresholding to reject noisy points. Through the KD tree associated with the leaf nodes of the model point cloud octree, search for the three points s_1, s_2, and s_3 that have the closest Euclidean distances to the point p_i; if the distance between p_i and the plane formed by s_1, s_2, and s_3 exceeds the threshold value E, then the corresponding point is rejected; otherwise, take the closest point among the three points s_j that has the closest distance to p_i as the corresponding point. As the corresponding point. The threshold value is $E=c\times d$, where c is the control coefficient and d is the average distance between neighboring points in the point cloud. In addition, the boundary noise points may also form multiple pairs of corresponding points, and two sets of corresponding pairs p_1 and q_1, p_2 and q_2 can be compared, and if Eq. (16) occurs, i.e., the difference between them is more than F, they are regarded as noise points, and they are also eliminated:

$$\left|dist\left(p_1-p_2\right)-dist\left(q_1-q_2\right)\right|\geq F \tag{16}$$

Although a large number of noisy points are eliminated by utilizing the Euclidean distance threshold, there are still noisy points in the corresponding point pairs. Considering that the point cloud to be matched and the model point cloud should have the same spatial topology although they are in different coordinate systems, there are rotations in addition to translations between the point clouds. Therefore, a threshold is set for the normal vector pinch angle of the matched point pairs to further eliminate the erroneous point pairs.

Given the point $\left(p_i,n_i\right)$, where n_i is the normal vector of the point p_i, find the approximate tangent plane of the point p_i by its neighboring set of points $\left\{\left(q_j,n_j\right)\right\}_{j=1}^{k}$ point's approximate tangent plane, and then find the approximate normal vector n_i of the p_i point that minimizes Eq. (17):

$$error=\sum_{j=1}^{k}\left(\left(q_j-p_i\right)n_i\right)^2 \tag{17}$$

Applying the least squares method, the following 3×3 matrix A can be obtained:

$$A=\sum_{j=1}^{k}\left(\left(q_j-p_i\right)^T\cdot\left(q_j-p_i\right)\right) \tag{18}$$

It can be shown that the eigenvector corresponding to the smallest eigenvalue of A can be used as an approximation of the normal vector n_i.

The normal vectors of each point in the two corresponding point sets are obtained by the above method. For any corresponding point pair p_i and q_j, their normal vectors are n_i and n_j respectively. The greater the difference between the normal vectors of the two, the smaller the cosine value of the angle, i.e., the smaller $n_i\cdot n_j$. Therefore, a threshold is set for the cosine of the angle of pinch of the vectors according to Eq. (19), i.e., pairs of points whose product of normal vectors is less than G are considered as noise points and are eliminated:

$$n_i\cdot n_j\geq G \tag{19}$$

III. B. 3) Algorithmic steps

The main steps of the improved point cloud alignment algorithm are as follows:

1) Establish an octree and KD tree multilayer index structure for the model point cloud Q.

2) Iterative initialization: select the initial target point set $P_0 = P$, set the maximum number of iterations $K_{\max}$, and give the normal threshold V.

3) Based on the coordinates $p_i(x_i, y_i, z_i)$ of each point p_i in the to-be-collimated point cloud P_k and the spatial location and size of the octree subcube enclosing the box (x, y, z, l), locate the octree where leaf node where the nearest point q_i is located.

4) Find the KD tree containing the local point cloud through the leaf nodes of the octree, and search for the nearest point of each point p_i in the data point set P_k based on the KD tree to get the corresponding point set Q_k.

5) Use Euclidean distance threshold and point-to-point distance difference to eliminate some noise points.

6) The wrong matched point pairs are eliminated according to the normal vector threshold.

7) Minimize Eq. (20) using quaternion method to find the rotation matrix R_k and translation vector T_k:

$$F(R_k, T_k) = \sum_{i=1}^{N} \left\| q_i - (R_k p_i + T_k) \right\|^2 \tag{20}$$

8) Obtain a new set of data points based on the rotation matrix R_k and the translation vector T_k: $P_{k+1} = R_k P_k + T_k$.

9) $R = R_k R$, $T = R_k T + T_k$, and repeat steps 3) to 8) until the distance between the previous closest point and the distance between the next closest point satisfies the condition: $d_k - d_{k+1} < t$ or the number of iterations is greater than a given value $K_{\max}$.

10) Use the transformation matrix parameters R and T to transform the initial target point cloud data to the coordinate system where the reference point cloud is located to complete the alignment of the point cloud data.

Let the model point cloud Q have N data points, the point cloud to be aligned P have M data points, the ratio of the total number of data points in the model point set N to the data points contained in a leaf node of the octree is K (segmentation parameter), and the depth of the octree of the model point cloud is h. It can be calculated that the number of points contained in each leaf node of the octree is N/K, the number of leaf nodes is K, and the octree is simplified to a full octree processing, and the octree depth can be calculated as:

$$h \geq \left| \log_8 K \right| + 1 \tag{21}$$

For a point cloud P to be aligned with M data points, the search time for the corresponding octree is $O(M \log_8 K)$; the search for the nearest point in the KD tree of the local model point cloud block is $O(M \log_2 (N/K))$. Therefore, the total time to search for the nearest neighbor is:

$$O\left(M \log_8 K + O\left(M \log_2 (N/K)\right)\right) \tag{22}$$

It is shown that the time for depth-first search of the nearest neighbor of the KD tree is $O(M \log_2 N)$ in the case of random distribution of instances, and $O(3MN^{2/3})$ in the worst backtracking case. Therefore, under the premise of guaranteeing the alignment accuracy, choosing an appropriate value of K and satisfying Eq. (23) will ensure that the improved algorithm outperforms the traditional KD-tree nearest-neighbor search algorithm under stochastic conditions:

$$M \log_8 K + M \log_2 N/K < M \log_2 N \tag{23}$$

To wit:

$$\log_8 K < \log_2 K \tag{24}$$

Obviously it is easy to satisfy the above equation that the larger the segmentation parameter K, i.e., the finer the segmentation of the point cloud model, the more time efficient it is, provided, of course, that the accuracy of the alignment needs to be guaranteed.

IV. Charged line safety distance modeling experiments

In this chapter, the experiments of visual sensor-based safety distance modeling of power line will be carried out to test the effectiveness of the point cloud alignment of the proposed method of 3D modeling of safety distance of power line in this paper and its effectiveness on the actual 3D modeling.

IV. A. Point cloud alignment effect analysis

In this section, experiments will be carried out on the open 3D point cloud dataset from Stanford University as a research object to compare the improved point cloud alignment algorithm proposed in this paper with the traditional ICP and KD-ICP algorithms.

IV. A. 1) Point cloud alignment evaluation criteria

In this paper, the Euclidean fitness score (MSE) is used to evaluate the accuracy and effectiveness of the algorithm. The Euclidean fitness score, which represents the sum of squares of the spacing from the output point cloud to the corresponding point pairs of the nearest target point cloud, uses the corresponding sum of squares of the nearest point distances as a criterion for judging the efficiency of the alignment, and if the smaller value of the sum of squares of the spacing is, it implies that the overlap rate and the accuracy of the alignment are higher, and the result expresses the proximity degree of the two point clouds. In addition, the timeliness and complexity of the algorithm can be measured by comparing the time used for the alignment.

IV. A. 2) Point cloud alignment results analysis

In this paper, Bunny, Dragon and Happy point cloud datasets are used for point cloud alignment in the experimental process. The accuracy of point cloud alignment between the improved point cloud alignment algorithm and the traditional ICP and KD-ICP algorithms is shown in Table 1. Compared with the ICP algorithm and KD-ICP algorithm, the algorithm in this paper can achieve a 2-3 orders of magnitude improvement in point cloud alignment accuracy, and the time spent in the alignment process is short and the alignment speed is fast, and the alignment effect is still able to maintain a certain degree of robustness for the point cloud set with a large amount of data. The time utilization and point cloud alignment accuracy are better than the traditional ICP and KD-ICP algorithms for comparison. In terms of alignment accuracy and running time, the algorithm in this paper has good feasibility and can maintain good alignment efficiency under the situation that the initial alignment accuracy is very different.

Table 1: Comparison of point cloud registration accuracy

Point cloud	ICP		KD-ICP		Algorithm of this article	
	Registration error(m)	Time(s)	Registration error(m)	Time(s)	Registration error(m)	Time(s)
Bunny	1.0327×10-5	96.82	2.0647×10-6	69.72	5.5907×10-8	6.58
Dragon	5.1872×10-6	20.47	1.3285×10-6	42.46	7.1115×10-8	4.93
Happy	1.5596×10-5	26.35	1.4326×10-6	58.28	1.2974×10-8	6.41

IV. B. Analysis of 3D modeling effect

IV. B. 1) Experimental Objects

The modeling object selected for this experiment is a part of the visual sensor area in the scene of a power distribution substation's power-carrying operation, and the basic image data required for modeling are obtained by using the tilt photography technique to take images of the visual sensor area. In order to improve the modeling effect, the image data set is preprocessed, so as to reduce the influence of image differences on the experimental results.

In order to compare the modeling effect of different methods, this paper firstly specifies the entity attributes of the modeled object scene, and the specific entity object attributes are shown in Table 2. For the following modeling entity objects, this paper adopts the form of triangles to cut the individual units, by splitting different objects in the scene into triangles of different sizes, so as to provide a benchmark for 3D modeling.

IV. B. 2) Comparative Analysis of 3D Modeling Effectiveness

In order to reflect the comparative nature of the experiment, the comparison index selected for this experiment is the modeling accuracy of different modeling methods, and the specific measurement index is the fitting degree between the elevation point curves under different modeling results, and the higher the degree of fitting, the higher the modeling accuracy of the representative method. In this experiment, traditional BIM modeling method and traditional GIM modeling method are selected as comparison objects, and the specific experimental results are shown in Fig. 1. Through the above elevation point curve fitting comparison results, it can be seen that when modeling the same scene object, the modeling accuracy of different methods is different. By observing the fitting degree of the curves, it can be seen that the elevation curve of the 3D model under the modeling method of this paper has a higher degree of fit with the original curve, which proves that the modeling accuracy of the method of this paper is higher.

Table 2: Modeling entity object properties

Column name	data type	length	Null or not null
Line number	char	24	Not null
Line ID	char	6	Not null
The starting region	numeric	13	Not null
Terminating area	numeric	15	Null
Model length	numeric	10	Null
Model width	numeric	13	Not null
Attitude angle	numeric	10	Not null
Model height	numeric	9	Null
Model ID	char	5	Null

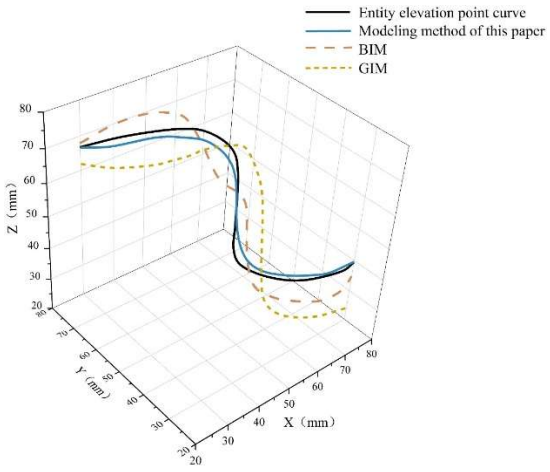

Figure 1: The comparison results of the fitting degree of elevation point curve

V. Charged line safety distance positioning method

In the above paper, this paper realizes the three-dimensional modeling of the safety distance of the strip line through the point cloud data alignment method. On this basis, this chapter will carry out the calculation of the safety distance of the strip line and complete the work of positioning the safety distance of the strip line based on the visual sensor.

V. A. Charged line safety distance calculation

In order to calculate the shortest distance from the energized line of the visual sensor to the surrounding equipment and the construction scope, the simplest method is to iteratively calculate the distance from each line point to each equipment point and take the portion of it that is less than the threshold value. The complexity of this algorithm is $O(n*m)$, and the amount of computation is very huge. In order to accelerate the selection of the nearest point, a 3D spatial division and retrieval of the 3D laser point cloud of each conductor is established. Subsequently, the laser points of each conductor are traversed.

Find whether the safety distance within the laser point of the power line is a safe distance for energized operation according to the safety distance specified in the safe operation regulations of the line.

KD tree is a kind of K-dimensional binary search tree, usually used to search for the distance to the nearest point, and each of its nodes contains two pointers, each pointer points to a sub-tree, is a kind of data structure in the space search. First of all, according to the x axis, calculate the average of all discrete points x value, with the average value of the two-dimensional space is divided into two subspaces, and then in these two subspaces, respectively, calculate the average of all the points y value, with the average value of the y to divide the two subspaces again. In the resulting subspace, divide it again according to the value of x. And so on until there is only one point in the divided subspace, this process corresponds to a binary tree. The branch nodes of a binary tree correspond to a line of division, and the leaf nodes correspond to a point, ensuring that there is no “pointless space” in the constructed KD tree. When there are n points, the time complexity of building the KD tree is. The process of searching for the nearest K points to a certain point using the KD tree is called KD tree search, and the method is to compare the nearest K points by calculating the Euclidean distance between all the points and a center point.

Usually, the search for neighboring points starts from the bottom of the tree, i.e., the small region of space, and gradually searches to the upper spatial region of the tree, so that the efficiency of spatial search for the nearest points can be improved better.

For each file of the point cloud to establish a k-d tree data structure, traversing each power line laser points, according to the safety distance specified in the safe operation of the line regulations to find the existence of equipment and facilities, construction sites, vegetation, buildings and other types of features within the scope of the point, if there is, it is recognized as a defective point location, and to generate a defect report to remind the construction staff.

V. B. Electric operation safety distance quantification

Through the data classification to obtain the whole site cloud information, the minimum safe distance real-time detection algorithm system, can manually measure the distance from the conductor to any device, automatically calculate the headroom distance to determine whether to meet the safety norms.

VI. Charged line safety distance positioning experiment

In order to verify the feasibility of this paper's visual sensor safety distance localization method for energized lines, it is necessary to carry out experiments in real application scenarios. Before the experiment, the electric field sensor needs to be calibrated, and the calibrated electric field sensor is able to represent the surface induced charge of the sensor at the measurement point through the output voltage. In addition, in order to get a more accurate uniform electric field this chapter according to the provisions of the national standard GB/T12720-91 design of the industrial frequency electric field calibration device, and the five electric field sensors (sensors 0 ~ 4) were calibrated. Finally, the feasibility of this paper's safety distance positioning method for energized lines is verified.

VI. A. Calibration of electric field sensors

During the experiment, the electric field sensor was placed on an insulated tray, and the height of the insulated tray was adjusted to ensure that the upper pole plate of the sensor was in the same plane as the lower surface of the calibration device. Then connect the oscilloscope to the output of the electric field sensor, and finally adjust the voltage U through the high-voltage generator U in the range of 0-10kV, because the uniform electric field produced by the calibration device E and the pole plate spacing D to meet the $E=U/D$ relationship, so the calibration device will produce a field strength of 0-100kV. The sensor calibration data are shown in Table 3.

Table 3: Sensor calibration data

Electric field intensity (V/m)	Sensor 0 (V/m)	Sensor 1 (V/m)	Sensor 2 (V/m)	Sensor 3 (V/m)	Sensor 4 (V/m)
0	0	0	0	0	0
10	404	448	470	400	398
20	925	885	884	803	873
30	1382	1358	1275	1286	1401
40	1801	1828	1772	1803	1884
50	2183	2415	2336	2285	2316
60	2633	2930	2888	2807	2754
70	3094	3361	3273	3224	3248
80	3535	3850	3747	3693	3716
90	3975	4338	4221	4161	4184
100	4416	4826	4696	4630	4652

The linear fitting curve for each electric field measurement system using the least squares method is shown specifically in Fig. 2. In the figure, (a)~(e) represent sensors 0~4 in sequence. The linear relationship between the voltage value $U(t)_i$ output from each electric field sensor and the uniform electric field E can be obtained by fitting the curve. The sensitivity coefficients of sensors 0 to 4 reach 44.045mV/(kV·m-1), 48.812mV/(kV· m-1), 47.441mV/(kV·m-1), 47.04mV/(kV·m-1), 46.815mV/(kV·m-1), which shows that the sensitivity coefficients of the sensors designed in this paper are closer and in good agreement. From the fitting degree, the fitting degree of sensor 0~4 reaches 0.9996, 0.9994, 0.9988, 0.9994, 0.9997, respectively, which has high linearity and meets the requirements of this paper.

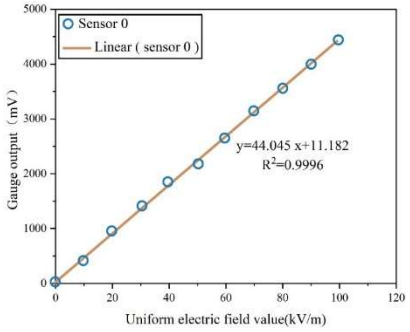

(a) Sensor 0

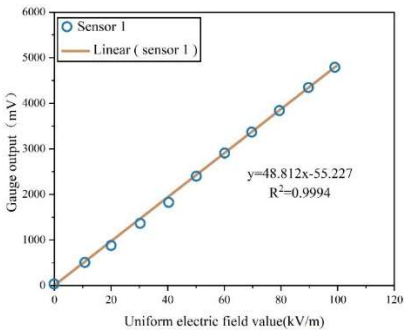

(b) Sensor 1

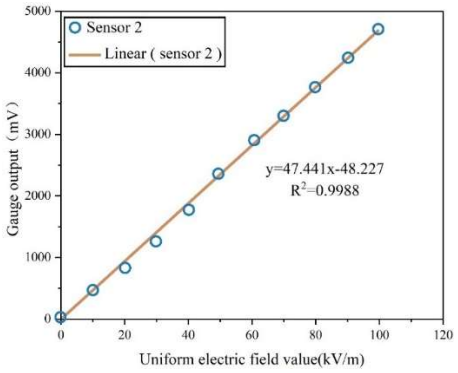

(c) Sensor 2

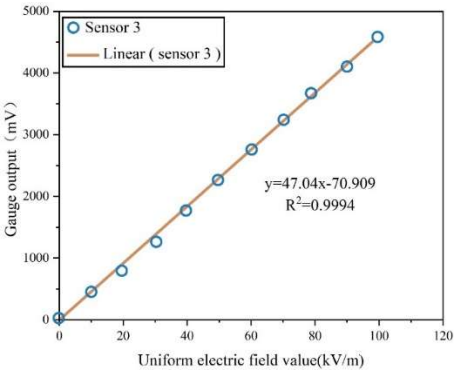

(d) Sensor 3

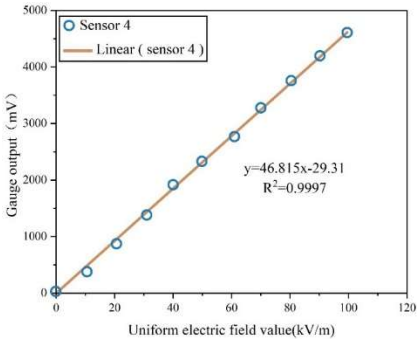

(e) Sensor 4

Figure 2: Data fitting results

VI. B. Analysis of Positioning Experiment Results

In order to prevent the high voltage from causing life safety problems for the experimenters, therefore, in this experiment, the measurement is only carried out in the voltage environment of 5kV. The following describes the measurement method and experimental steps for each localization parameter.

1) Elevation angle measurement

Measurements were made by placing the detector on an insulated table with a height of h1 = 0.25 m above the ground and on a cardboard box with a height of h2 = 0.15 m above the ground, respectively. The schematic of the optimized detector is shown in Fig. 3. A spherical coordinate system is established at the detector's center of origin O, with the line connecting sensors 0 and 1 as the X axis and the line connecting sensors 0 and 2 as the Y axis. Among them, four one-dimensional circular capacitive IFE sensors with an inductive polar plate radius of 1.5 cm and a thickness of 1.5 mm are uniformly arrayed in the same circumference, while one sensor is also arranged in the center; the radius of the array is 20 cm. In this experiment, by replacing h2 with h1 without changing ρ, different elevation angles can be measured under the condition of no change in ρ, θ.

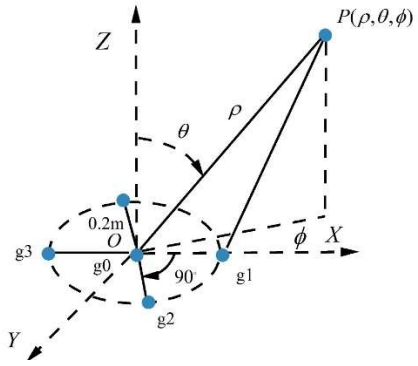

Figure 3: Schematic diagram of the optimized detector

2) Distance Measurement

In order to obtain different distances between the detector center and the field source, the detector can be placed on an insulated table, carton and dragged in the direction of OX insulated table, carton, so that the detector center and the distance from the field source changes. Measurement points for 10, 35, 110kV corresponding to the safety distance of 1.5 times the position of 1.05, 1.5, 2.25 m. The output value of each sensor and the measurement error and other positioning experimental data are shown in Table 4, in which the measurement error of the actual location of the field source parameter subtracted from the absolute value of the measurement of the position parameter. As can be seen from the table:

(1) Under the experimental conditions of this paper, when the detector is located at the 10kV alarm distance, the ranging error is 0.18m, the elevation error is 6.8°, and the azimuth error is 4.57°.

(2) When the detector is located at the 35kV alarm distance, the measurement error is 0.2m, the elevation error is 4.8°, and the azimuth error is 5.14°.

According to the alarm distance is 1.5 times of the safety distance, it can be seen that the allowable range of distance error is within 0.35m for 10kV and 0.5m for 35kV, which indicates that the visual sensor proposed in this paper meets at least the safety distance warning requirements of 10kV and 35kV for the safety distance localization method of the energized line. When the detector distance from the ground is reduced from h1 to h2, the measured value at the same distance decreases, because the field source is closer to the ground, and the electric field lines reach the detector with a non-uniform electric field. However, the localization method of this paper can still be used. It should be noted that when the azimuth angle of 90 °, 270 ° will not be able to get a feasible solution, this time can only be used for distance and elevation angle calculation.

When the detector is located in the 110kV alarm distance distance error reached 1.14m, elevation error reached 35.47 °, azimuth error reached 23.71 °, and even appeared to be unable to calculate the distance, elevation angle of the situation (shown in the table with "×"). This is because the experiment uses a 5kV field source, when the detector is too far away from the field source when the sensor receives a weak signal, the value between the sensors is too close to each other, resulting in a slight deviation of the sensor output value from the theoretical value will also bring about a large measurement error, or even the appearance of no solution. The experimental ranging error is higher than the simulated ranging error by 8.4-11.5%, which is due to factors such as temperature, humidity, edge effect, and operation error on the surface of the sensor sensing plate.

Table 4: Location experimental data

Field source coordinate P	Sensor 0 (kV/m)	Sensor 1 (kV/m)	Sensor 2 (kV/m)	Sensor 3 (kV/m)	Sensor 4 (kV/m)	Measurement error $P(\rho,\theta,\phi)$
(1.05,35.52,0)	3.3	4.01	3.16	2.6	3.13	(0.13,4.63,1.16)
(1.05, 35.52,60)	3.3	3.68	3.93	2.88	2.69	(0.16,8.6,4.57)
(1.05,42.55, 0)	2.77	3.58	2.65	2.1	2.64	(0.18,6.15,2.29)
(1.5,24,0)	1.34	1.49	1.3	1.24	1.28	(0.17,1.67,5.14)
(1.5,24,30)	1.34	1.4.4	1.36	1.21	1.25	(0.2,4.8,3.9)
(1.5,28.25,0)	1.07	1.25	1.04	0.9	1.05	(0.19,4.8,1.72)
(2.25,15.73,0)	0.45	0.47	0.43	0.42	0.43	(0.47,35.47,0)
(2.2.5,15.73,100)	0.45	0.46	0.47	0.45	0.43	(×,×,23.71)
(2.25,18.39,0)	0.35	0.37	0.33	0.32	0.33	(1.14,6.29,11.86)

VII. Conclusion

After fusion of multiple data from visual sensors and denoising of inspection visual letters, this paper proposes a point cloud alignment and power line safety distance calculation method based on octree and KD tree index based on hierarchical algorithm to realize three-dimensional modeling and positioning of power line safety distance.

Carry out the experiments on the safe distance modeling of power lines to test the effectiveness of the three-dimensional modeling method of the safe distance of power lines in this paper. In the analysis of point cloud alignment results, the improved point cloud alignment algorithm in this paper can achieve 2~3 orders of magnitude improvement compared with ICP algorithm and KD-ICP algorithm, and has faster alignment speed and higher alignment accuracy. At the same time, according to the comparison results of elevation point curve fitting, the modeling accuracy of the 3D modeling method of safety distance of power line in this paper is better than that of the traditional BIM modeling method and the traditional GIM modeling method, and the elevation point curve of the 3D model has a higher degree of fitting with the original curve.

Carry out the experiments on the positioning of the safety distance of the charged line in the actual application scenario to verify the feasibility of the positioning method of the safety distance of the charged line in this paper. According to the provisions of the national standard GB/T12720-91, the industrial frequency electric field calibration device is designed, and five electric field sensors (sensors 0~4) are calibrated respectively. In the experiment, 10kV, 35kV alarm distance when the distance measurement error is 0.18m, 0.2m, respectively, are lower than the distance error allowable range. Although the experimental ranging error is higher than the simulated ranging error by 8.4-11.5% due to the temperature of the sensor sensing plate surface and operation error, it meets the safety distance warning requirements in practical application scenarios on the whole.

Funding

Project Fund No.: State Grid Jiangsu Electric Power Co., LTD. (No.: J2024124): Research on online Supervision Technology of key power grid infrastructure operations based on smart wearable devices.

About the Author

Fei Shen was born in 1978 in Taicang, Jiangsu. Male, Han ethnicity. I am currently employed State Grid Jiangsu Electric Power Co., Ltd. Taizhou Power Supply Branch in Taizhou, Jiangsu. My main research direction is power grid infrastructure project management.

Yurong Zhang was born in 1980, female, Han ethnicity, Jiangsu Taizhou person. I am currently employed at State Grid Jiangsu Electric Power Co., Ltd. Taizhou Power Supply Branch in Taizhou, Jiangsu. My main research direction is power grid engineering management.

Bin Qian was Born in Taizhou in 1981, male, Han nationality, I am currently employed at State Grid Jiangsu Electric Power Company Taizhou Power Supply Branch in Taizhou, Jiangsu. My main research direction is power grid engineering management.

References

[1] Balametov, A., Halilov, E., & Isayeva, T. (2018). Extra high voltage transmission line operation simulation using the actualcorona-loss characteristics. Turkish Journal of Electrical Engineering and Computer Sciences, 26(1), 479-488.

[2] Fişcă, M., Abrudean, M., Mureşan, V., Clitan, I., Ungureşan, M. L., Motorga, R., & Ceuca, E. (2022). Modeling and Simulation of High Voltage Power Lines under Transient and Persistent Faults. Mathematics, 11(1), 21.

[3] Gracheva, E., Toshkhodzhaeva, M., Rahimov, O., Dadabaev, S., Mirkhalikova, D., Ilyashenko, S., & Frolov, V. (2020). Modeling the Reliability of High-Voltage Power Transmission Lines Taking into Account the Influence of the Parameters of a Sharply Continental Climate. International Journal of Technology, 11(8).

[4] Yang, B., Tang, J., Dong, X., Li, S., Gu, R., & Hao, J. (2023). Power inspection design by internet of things and RFID technology in smart city. Microprocessors and microsystems, 96, 104510.

[5] Gauce, D., Lektauers, A., Solovjova, I., Grants, R., Kolosovs, D., & Litvinenko, A. (2023). Application of digital twin in medium-voltage overhead distribution network inspection. Remote Sensing, 15(2), 489.

[6] Zhang, Y., Xie, Q., Zhuang, C., Li, C., & Zhang, P. (2023). Application of power grid equipment digital and intelligent technology in operation and maintenance. Frontiers in Energy Research, 11, 1231815.

[7] Miroshnyk, O., Moroz, O., Shchur, T., Chepizhnyi, A., Qawaqzeh, M., & Kocira, S. (2023). Investigation of Smart Grid Operation Modes with Electrical Energy Storage System. Energies, 16(6), 2638.

[8] Piechoczek, E., & Gela, G. (2024). Procedures for the Safe Operation of Helicopters in an Energized Wire Environment. Safety & Defense, 10(1), 57-67.

[9] Jia, J., Zhang, F., Guo, R., Cao, L., & Lin, H. (2021, October). Research on Live working Robot technology for 500kV Overhead transmission line. In 2021 IEEE 5th Information Technology, Networking, Electronic and Automation Control Conference (ITNEC) (Vol. 5, pp. 474-478). IEEE.

[10] Jeong, S., Kim, M. G., Kim, J. H., & Oh, K. Y. (2023). Thermal monitoring of live-line power transmission lines with an infrared camera mounted on an unmanned aerial vehicle. Structural Health Monitoring, 22(6), 3707-3722.

[11] Chen, Y., Wang, Y., Tang, X., Wu, K., Wu, S., Guo, R., ... & Dong, E. (2023). Intelligent power distribution live‐line operation robot systems based on stereo camera. High Voltage, 8(6), 1306-1318.
[12] Ziming, S., Kai, L., Ting, L., Bin, X., Xi, Z., & Bingqiang, W. (2017, May). Research on security distance of live working on distribution line at high altitudes. In 2017 1st International Conference on Electrical Materials and Power Equipment (ICEMPE) (pp. 686-690). IEEE.
[13] Lei, T., Xie, Z., Wang, K., Zhong, L., & Chen, D. (2021, August). Design of high voltage live operation robot system. In 2021 International Conference on Wireless Communications and Smart Grid (ICWCSG) (pp. 473-476). IEEE.
[14] Lei, L., Shuai, L., Nan, W., Xi, W., & Yujian, D. (2022, July). Safe distance test and altitude correction for live working with helicopter sling method on±400kV DC transmission. In IET Conference Proceedings CP803 (Vol. 2022, No. 5, pp. 235-239). Stevenage, UK: The Institution of Engineering and Technology.
[15] Zhang, B., Dai, R., Ma, W., Wu, H., Zhi, L., Chen, Y., & Zhang, Y. (2019). Simulation calculation of electric field protection for live working on Ultra‐high voltage transmission line. The Journal of Engineering, 2019(16), 2042-2046.
[16] Ruan, H., Zou, D., Wang, W., He, Z., & Yan, Y. (2020). Online Live Working Safety Monitoring and Early Warning Based on Spatial Cross‐Border Prevention. IEEJ Transactions on Electrical and Electronic Engineering, 15(6), 881-893.
[17] Li, H., Ding, Z., Li, L., Xu, D., & Wang, D. (2023, October). Application of Large-scale Point Cloud using Distance-based Monitoring for Live-line Work on 220kV Transmission Lines. In 2023 9th Annual International Conference on Network and Information Systems for Computers (ICNISC) (pp. 378-383). IEEE.
[18] Wu, S., Wang, L., Wang, G., Zu, S., Gao, J., & Song, B. (2025). A visual and automated calculation method for hazardous areas of live-line work based on point cloud. IEEE Sensors Journal.
[19] Wang, Y., Zhang, H., Lv, Q., Gao, Q., & Yi, M. (2023). Measurement of combined gap in whole process of transmission lines' live working based on 3D laser point cloud. Archives of Electrical Engineering, 72(3).
[20] Li, J., Shuang, F., Huang, J., Wang, T., Hu, S., Hu, J., & Zheng, H. (2023). Safe distance monitoring of live equipment based upon instance segmentation and pseudo-LiDAR. IEEE Transactions on Power Delivery, 38(4), 2953-2964.
[21] Fernandes, L. A. (2024). Editorial to the Special Issue "Vision Sensors: Image Processing Technologies and Applications". Sensors, 24(6), 1803.
[22] Yang Feng,Hengyi Lv,Hailong Liu,Yisa Zhang,Yuyao Xiao & Chengshan Han. (2020). Event Density Based Denoising Method for Dynamic Vision Sensor. Applied Sciences,10(6).
[23] Minglei Li,Mingfan Li,Min Li & Leheng Xu. (2025). Building Lightweight 3D Indoor Models from Point Clouds with Enhanced Scene Understanding. Remote Sensing,17(4),596-596.
[24] Elizeu Martins Oliveira Junior,Daniel Rodrigues Santos & Giovana Angélica Ross Miola. (2022). A New Variant of the ICP Algorithm for Pairwise 3D Point Cloud Registration. American Academic Scientific Research Journal for Engineering, Technology, and Sciences,85(1),71-88.
[25] Honglu Zhu,Xi Zhang,Ji Wu,Siyu Hu & Yuhang Wang. (2025). A novel solar irradiance calculation method for distributed photovoltaic power plants based on K-dimension tree and combined CNN-LSTM method. Computers and Electrical Engineering,122,109990-109990.